CHAPTER 12

Ultraviolet-Visible Spectroscopy

Bert M. Weckhuysen

Department of Inorganic Chemistry and Catalysis, Debye Institute, Utrecht University, Sorbonnelaan 16, 3584 CA Utrecht, The Netherlands

CONTENTS

1. INTRODUCTION

Spectroscopy in the ultraviolet (UV), visible (Vis) and near-infrared (NIR) region of the electromagnetic spectrum is often called electronic spectroscopy because electrons are transferred from low-energy to high-energy atomic or molecular orbitals when the material is irradiated with light [1]. Such electron transfer processes may take place in transition metal ions (d-d transitions and ligand-to-metal or metal-to-ligand charge transfer transitions), and inorganic and organic molecules (mainly $n \rightarrow \pi^*$ and $\pi \rightarrow \pi^*$ transitions). They are responsible for the color of matter.

Spectroscopic investigations of solutions, gas phase and individual crystals usually take place in transmission, but it is very difficult to obtain transparent films of powders and solids (e.g., heterogeneous catalysts), making transmission experiments almost impossible. Alternatively, diffuse reflected light can be collected and this technique has been named diffuse reflectance spectroscopy (DRS) [2]. One of the advantages of DRS is that the obtained information is directly chemical in nature since outer shell electrons of the transition metal ions are probed. This provides information about the oxidation state and coordination environment of transition metal ions in catalytic solids. The same holds for the nature of adsorbed species and different hydrocarbon species can be investigated. Furthermore, DRS is quantitative and can be used under *in-situ* conditions. The main disadvantage of the technique is that DRS spectra are complex, and usually encompass several broad and overlapping bands. In order to avoid biased spectral analysis, chemometrical techniques need to be employed. This is especially important for *in-situ* time-resolved DRS studies because of the extensive spectroscopic database to be handled.

This chapter starts with a short overview of the principles of DRS. Theoretical as well as practical aspects will be discussed. The next section focuses on three examples in order

ISBN: 1-58883-026-8/$35.00

In-situ Spectroscopy of Catalysts
Edited by B. M. Weckhuysen

to illustrate the potential and limitations of *in-situ* UV-Vis-NIR spectroscopy. The first example deals with Cr/Al_2O_3 alkane dehydrogenation catalysts and the use of different *in-situ* DRS set-ups for studying heterogeneous catalysts under reaction conditions. The second example illustrates the use of *in-situ* DRS spectroscopy to monitor the crystallization process of MeAPO-5 molecular sieves at high pressures and temperatures. The third example shows how *in-situ* DRS can be used to obtain insight in the reaction mechanism of the NO decomposition over Cu-ZSM-5 catalysts. The chapter ends with some concluding remarks.

2. PRINCIPLES OF DIFFUSE REFLECTANCE SPECTROSCOPY IN THE UV-VIS-NIR REGION

The interaction of light of the UV-Vis-NIR region with catalytic solids is considered to be a complex process due to absorption and scattering phenomena. These phenomena are largely overcome by the application of techniques such as DRS spectroscopy and photoacoustic spectroscopy (PAS). The technique of PAS will not be treated in this textbook because its use in the field of catalysis is rather limited [1]. It is also important to mention that only in limited cases, solids (more specifically zeolites) have been pressed in thin wafers of high transmittance so that UV-Vis-NIR spectroscopy was performed in transmission mode [3–6]. Although transmission mode certainly has advantages, almost all UV-Vis-NIR investigations in the catalysis field have been conducted in diffuse reflection mode due to the high absorption and scattering of the materials. In what follows, we will briefly discuss the principles of DRS. For detailed explanations and in-depth discussions, we refer to the seminal textbook of Kortüm [7] and to several excellent review papers [8–11].

2.1. Theoretical Considerations

DRS is based on the reflection of light by a powdered sample, and the dimensions of the individual particles in such powdered sample are comparable to the wavelength; i.e., 0.2–3 μm [1]. This makes it impossible to distinguish the phenomena of reflection, refraction and diffraction; the light is scattered. There are two extreme situations of reflection: specular and diffuse reflection (Figure 1). In the case of specular reflection from a smooth and non-absorbing medium, the light beam is reflected under the same angle by the surface as that of the incoming light beam. On the other hand, diffuse reflected light from a non-absorbing medium involves photons, which are scattered in all directions. Three different regimes can be distinguished: (1) single scattering; (2) multiple scattering; and, (3) dependent scattering. The first type arises when scattering centers are sufficiently apart that each is illuminated only by light particles not previously scattered, and on the average, there is no phase relationship between the photons scattered from neighboring particles. In the case of multiple scattering, the scattering centers are still far enough apart that they may be treated as independent, but each center is now illuminated by photons scattered from adjacent particles. Dependent scattering arises when, in addition to multiple scattering, phase coherence exists between scattered photons from adjacent centers. As a rule of thumb, one can say that dependent scattering is present, if the average distance (d) between scattering centers is less than three times the particle diameter (3D) (Figure 2).

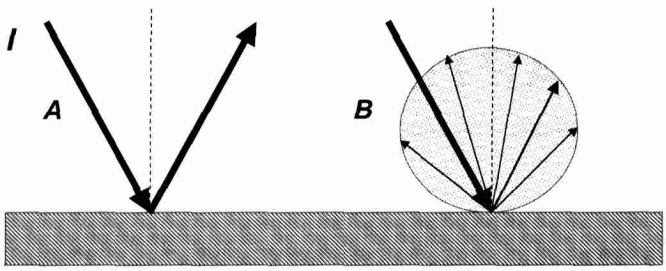

Figure 1. Light scattering at smooth non-absorbing surfaces after irradiating the particle surface with light I: specular reflected light (A) and diffuse reflected light (B).

The division of light scattering systems into the above three regimes determines the theoretical approach necessary to describe the scattered light intensity. For single and multiple scattering, the absence of phase coherence ensures that the total scattered light intensity is merely the sum of the intensities of the individual scatterers. Both types of scattering can be mathematically treated in a rather easy way. In contrast, when the particles become so tightly packed that phase coherence becomes important, amplitudes rather than intensities must be summed. This is the case for heterogeneous catalysts because they are always investigated in the form of densely packed powders. Then, the radiation transfer theory has to be called in, which sets out to solve the radiation transfer equation:

$$\frac{-dI}{\kappa \cdot \rho \cdot dS} = I - \frac{j}{\kappa} \qquad (1)$$

with I, the incident light intensity of a given wavelength; dI/dS, the change of the intensity with the path length dS; ρ, the density of the medium; κ, an attenuation coefficient corresponding with the total radiation loss due to absorption and scattering; and j, the scattering coefficient, which is defined

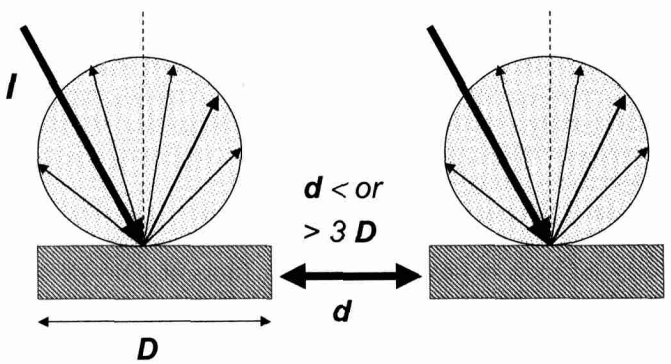

Figure 2. Rule of thumb discriminating between single, multiple and dependent scattering: D is the diameter of the particles and d is the distance between two adjacent particles.

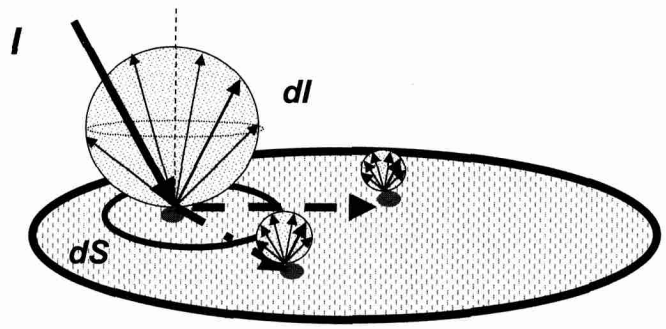

Figure 3. Scheme of dependent scattering.

through the function $j(\theta, \phi)$:

$$j(\theta, \phi) = \frac{\kappa}{4\pi} \int_0^{\pi} \int_0^{2\pi} p(\theta, \phi; \theta', \phi')\, I(\theta', \phi') \sin\theta' \cdot d\theta' \cdot d\phi' \quad (2)$$

Eq. (1) is schematically illustrated in Figure 3. This equation can be solved by introducing some simplifications, which are related to specific experimental conditions. These ideas, first suggested by Schuster and later developed by Kubelka and Munk, simplify the solution of the radiative transfer equation (Eq. (1)), known as the Schuster-Kubelka-Munk (S-K-M) theory.

In this S-K-M theory, the incident and scattered light flux are approximated by two fluxes I and J, which are perpendicular to the surface of the powdered sample, but in opposite directions (Figure 4). I is the flux of monochromatic diffuse illumination, whereas J is the flux of diffusively scattered light. If the sample is infinitely thick, the diffuse reflection of the sample (R_∞) is related to an apparent absorption (K) and apparent scattering coefficient (S) via the Schuster-Kubelka-Munk (S-K-M) or Kubelka-Munk (K-M) function:

$$F(R_\infty) = \frac{(1 - R_\infty)^2}{2R_\infty} = \frac{K}{S} \quad (3)$$

Eq. (3) is valid under the following conditions:

(a) diffuse monochromatic irradiation of the powdered sample;
(b) isotropic light scattering;
(c) an infinite layer thickness;
(d) a low concentration of absorbing centers;
(e) a uniform distribution of absorbing centers;
(f) the absence of fluorescence.

R_∞ is experimentally measured as the light intensity reflected from the powdered sample divided by the light intensity reflected from an ideally white reference standard. K and S are characteristic of the sample under investigation, and the true absorption coefficient α_ν and true scattering coefficient σ_ν at frequency ν are related to K and S via:

$$\alpha_\nu = \eta \cdot K \text{ and } \sigma_\nu = \chi \cdot S \quad (4)$$

Values of η and χ are plotted and tabulated for a range of K/S values, and it is shown that in the limit of small absorptions η and χ are equal to 1/2 and 4/3, respectively. It follows from Eq. (3) and (4) that:

$$\frac{\alpha_\nu}{\sigma_\nu} = \frac{(1 - R_\infty)^2}{2R_\infty} \cdot \frac{\eta}{\chi} \quad (5)$$

Equations 4 and 5 are introduced by Klier [12], and the ratio η/χ is fairly constant and equal to 3/8 for values of K/S between 0 and 0.3. For strongly absorbing solids (K/S > 0.3 or $R_\infty < 0.5$), η/χ decreases. Thus, at low concentrations of absorbing centers, Eq. (3) is a good representation of the absorption spectrum, and allows a quantitative determination of an absorption center in a catalytic solid according to:

$$F(R_\infty) = [(1 - R_\infty)^2/(2R_\infty)] = K/S = \alpha C/S = k \cdot C \quad (6)$$

When, at a given wavelength λ, S is constant, Eq. (6) gives a linear relation between $F(R_\infty)$ and the absorption center concentration, C. The coefficients α and k are proportionality constants.

As mentioned above, the S-K-M equation is only valid under well-defined conditions. Conditions (a), (b) and (d) are most closely met when the medium consists of densely packed particles containing low amounts of absorption centers. The infinite thickness criterion (condition (c)) is usually reached for sample layers of 5 mm thickness, although some catalyst supports (e.g., Cab-O-Sil Cabot and Aerosil Degussa) may need thicker layers. For *in-situ* studies on heterogeneous catalysts, specially designed cells are necessary with silica windows with extremely low OH contents since these species give rise to overtone bands in the NIR region. This may hamper the observations of absorption bands of supported transition metal ions in the reduced state. It is also advisable to sieve the catalytic solid and to work with fractions of the same size range.

Finally, it is important to stress that the scattering power of

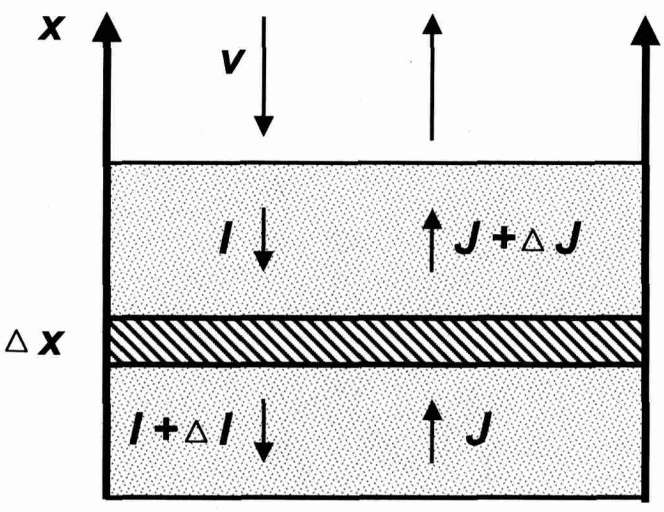

Figure 4. The Schuster-Kubelka-Munk approximation: the incident and remitted light fluxes are approximated by two opposite fluxes I and J, perpendicular to the surface of the infinitely thick sample layer.

a catalyst system, as expressed by S, is not of any importance provided that it is not a function of the wavelength λ or frequency ν. If S is frequency dependent, then distortions, appearing mostly as a smoothly shifting baseline, will result since K/S is measured as a function of ν. Fortunately, a strong frequency dependence of S is not expected for particles, which are large in comparison to the wavelength of the scattering radiation. The frequency dependence of S can be expressed as:

$$S = \nu^{\alpha} \tag{7}$$

Parameter α approaches 0 for particle sizes much larger than the wavelength λ. It is approximately 1 for particle sizes of the order of wavelength λ. It attains values between 2 and 4, increasing with decreasing particle size, which is, in any case, smaller than the wavelength λ. The situation $\alpha = 4$ corresponds to single scattering at small particles, which is important for Raman spectroscopy.

2.2. *In-situ* Instrumentation

In a DRS spectrum, the ratio of the light scattered from an infinitely thick layer and the scattered light from an ideal non-absorbing reference sample is measured as a function of the wavelength [12]. The illumination of powdered samples by incident radiation leads to diffuse illumination of the material. This incident light is then partially absorbed and partially diffusively scattered by the catalyst particles. The light sources for DRS measurements are a H_2 or D_2 lamp for UV irradiation (160–375 nm) and a tungsten filament lamp for the Vis-NIR region (350–2500 nm), while the reflected light is usually detected with a photo-multiplier tube (PM) in the UV-Vis region (200–800 nm), and a PbS detector in the NIR region (750–3000 nm). There are now also photodiode arrays (PDA) and charge coupled device (CCD) detectors for the range 200–1100 nm, allowing the acquisition of the whole spectra at once.

There are three different ways to measure *in-situ* DRS spectra of catalytic solids under working conditions:

(1) An integration sphere. This attachment collects almost all of the light scattered (> 95%) over a wide range of wavelengths, including the NIR range from the catalyst sample and from a reference standard, and the detectors are placed on top of the integration sphere. An *in-situ* DRS cell is placed in front of this classical setup, as illustrated in Figure 5. Because the integration sphere must scatter the light and not absorb it, it is coated with a perfectly white material (MgO, $BaSO_4$, Spectralon®, etc.). In this way, a negligibly small amount of specular reflection is included, but precautions can be taken to minimize the specular component. This method offers a good light yield and the option to record spectra in the NIR region. Unfortunately, no commercial *in-situ* DRS cells for such integration sphere are available. This has forced researchers to design their own cells. An example of such design used in our laboratory is shown Figure 6. It consists of a small container with an internal volume consisting of walls of high-purity quartz of 5 mm thickness [13]. The cell can be placed in a heating mantle, controlled by a Eurotherm thermoregulator. The flat front window of the cell placed in front of the integration sphere of the spectrometer allowed the recording of *in-situ* spectra of a catalyst in liquid-phase reactions at high temperatures and pressures. Other designs of such *in-situ* cells can be found in the literature. Nice examples are

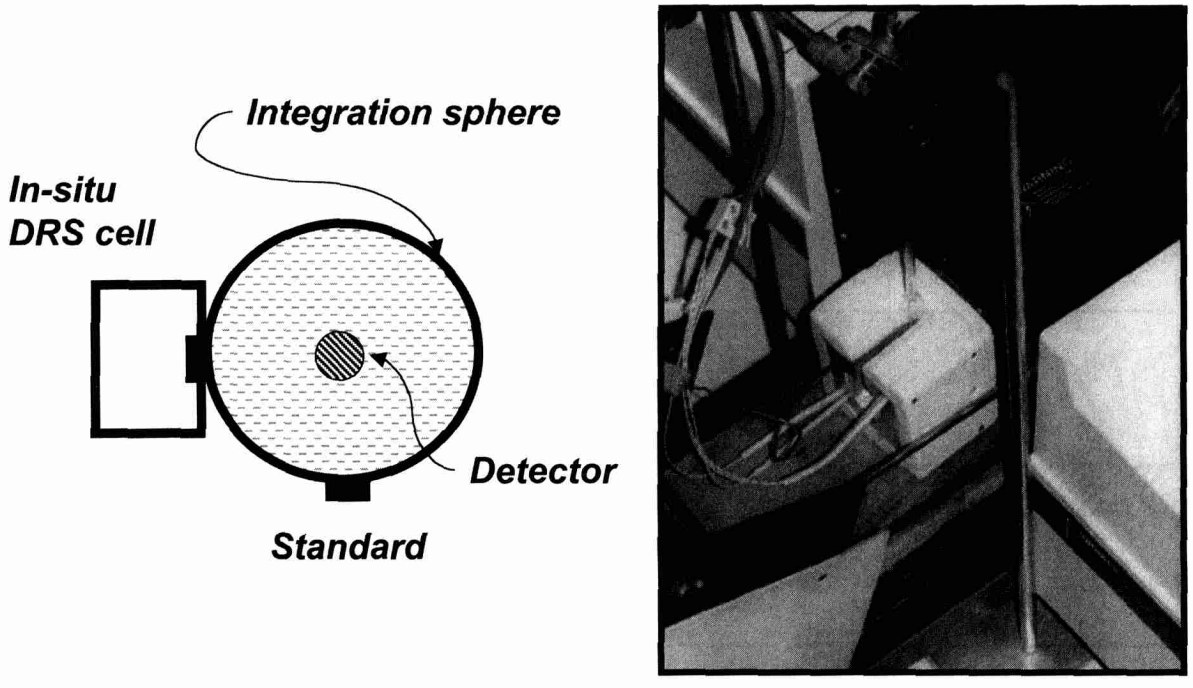

Figure 5. Schematic overview and picture of an UV-Vis-NIR spectrophotometer equipped with an integration sphere. The *in-situ* DRS cell is placed in front of the integration sphere.

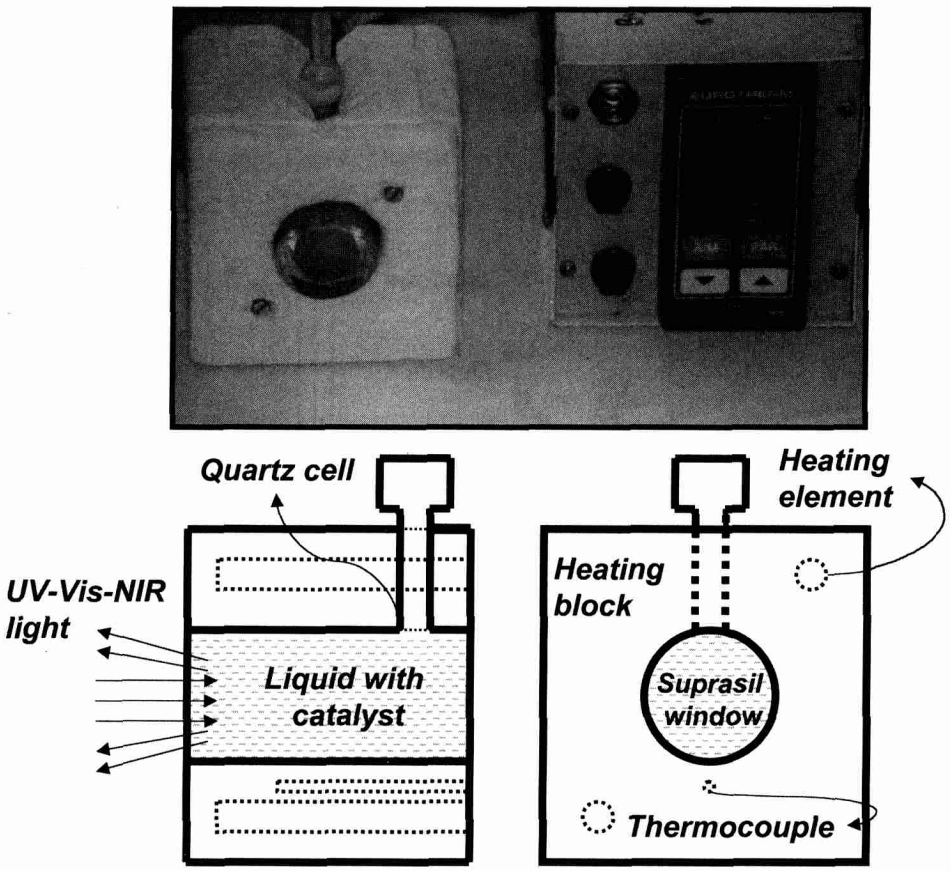

Figure 6. Scheme and picture of an *in-situ* DRS cell for measuring solids operating in liquid-phase reactions at elevated temperatures and pressures.

the *in-situ* DRS cells designed by Melsheimer et al. [14, 15]. Their cells allow the measuring of gas-phase reactions over catalytic solids in the range of 250–2500 nm, making use of a spacer to bridge the distance between integration sphere and microreactor. Spectra with high signal-to-noise ratio of catalysts heated up to 450°C were obtained.

(2) A diffuse reflectance accessory consisting of two ellipsoidal mirrors so that about 20% of the diffusively reflected light is collected and the specular component is minimized [16]. The set-up is illustrated in Figure 7. In conjunction with this so-called Praying Mantis diffuse reflectance attachment, a stainless steel reaction chamber can be used for low- or high-pressure *in-situ* DRS measurements. This system has three gas ports for evacuation of the chamber and/or for introducing gas, while the temperature near the catalyst bed can be controlled by an electronically steered heating system and circulating tap water for cooling the outer section of the reaction chamber. This chamber can be used under dynamic conditions and the gases can be on-line analyzed by gas chromatography or mass spectrometry. This system has been studied in detail by the groups of Wachs [17–19], Iglesia/Bell [20–22] and Weckhuysen [23–25].

(3) A fibre optics attachment equipped with a high-temperature probe easily insertable in a catalytic reactor (Figure 8) [26–28]. This *in-situ* DRS set-up collects only a small fraction of the reflected light and the data lacks reproducibility over long measuring times because of single beam design. In addition, there is no optical fibre available for the NIR range (above 1100 nm). The advantages, however, are: (1) the elegant coupling to a catalytic reactor, allowing the performance of on-line *in-situ* measurements; and, (2) the measurement of spectra in a time-resolved manner since the light is detected with a CCD or PDA detector. Several groups have tried to combine this approach with other *in-situ* spectroscopic techniques. The following combined *in-situ* spectroscopies have been investigated: DRS-EPR [29, 30] and DRS-Raman [31]. The latter set-up is illustrated in Figure 9. An experimental set-up combining *in-situ* DRS, Raman and energy-dispersive or quick-EXAFS is currently under construction in our laboratory [32]. A schematic drawing of this set-up is shown in Figure 10.

2.3. Practical Considerations

The choice of a proper reference standard and coating material for the integration sphere is also crucial for reliable *in-situ* DRS measurements. Excellent reference materials are totally reflecting over an as-wide-as-possible wavelength range. All

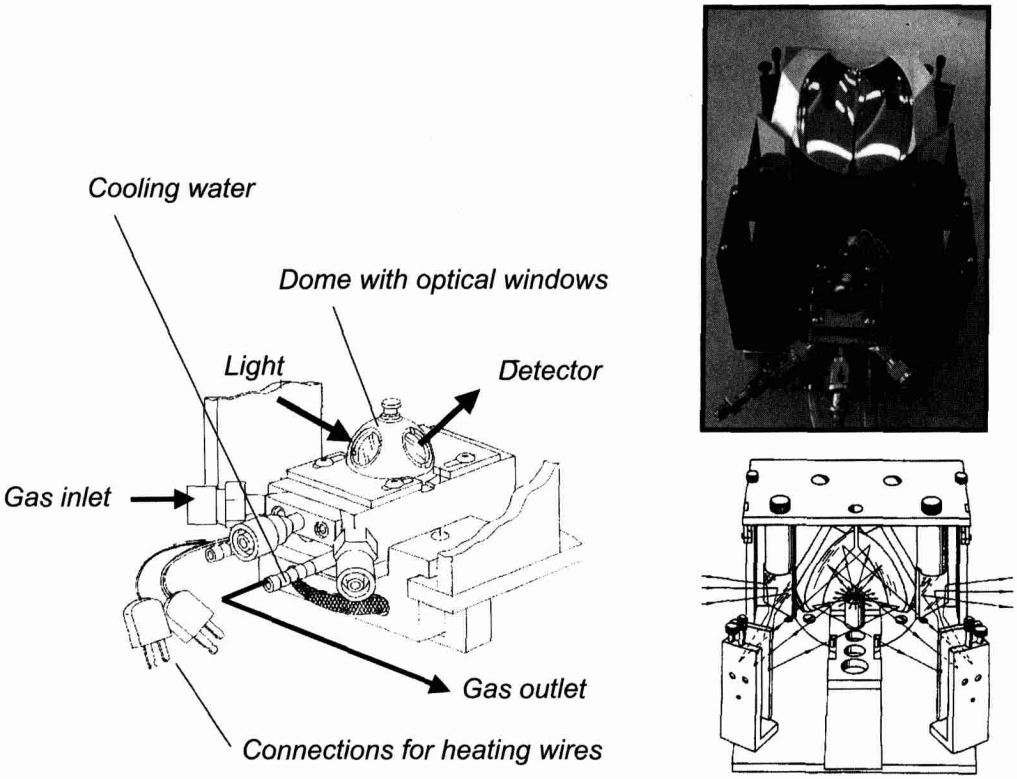

Figure 7. Scheme and picture of the Praying Mantis UV-Vis set-up for measuring catalytic solids operating in gas-phase reactions at elevated temperatures and ambient pressures. Both the Praying Mantis diffuse reflection attachment and the stainless steel reaction chamber are shown.

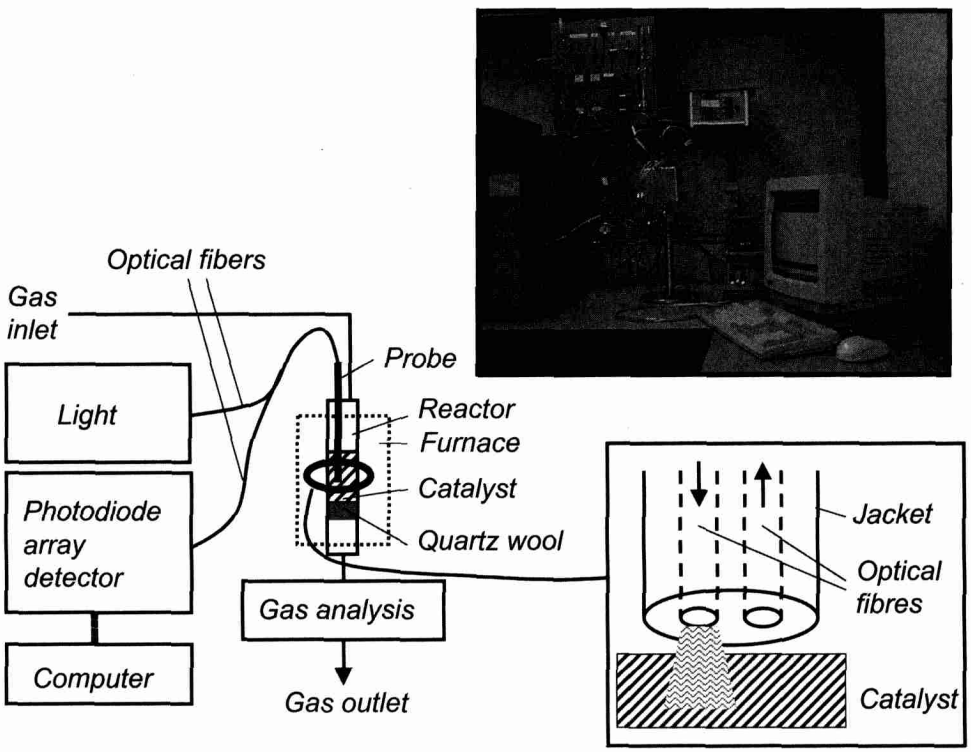

Figure 8. Scheme and picture of the fiber optic UV-Vis set-up for measuring catalytic solids operating in gas-phase reactions at elevated temperatures and ambient pressures.

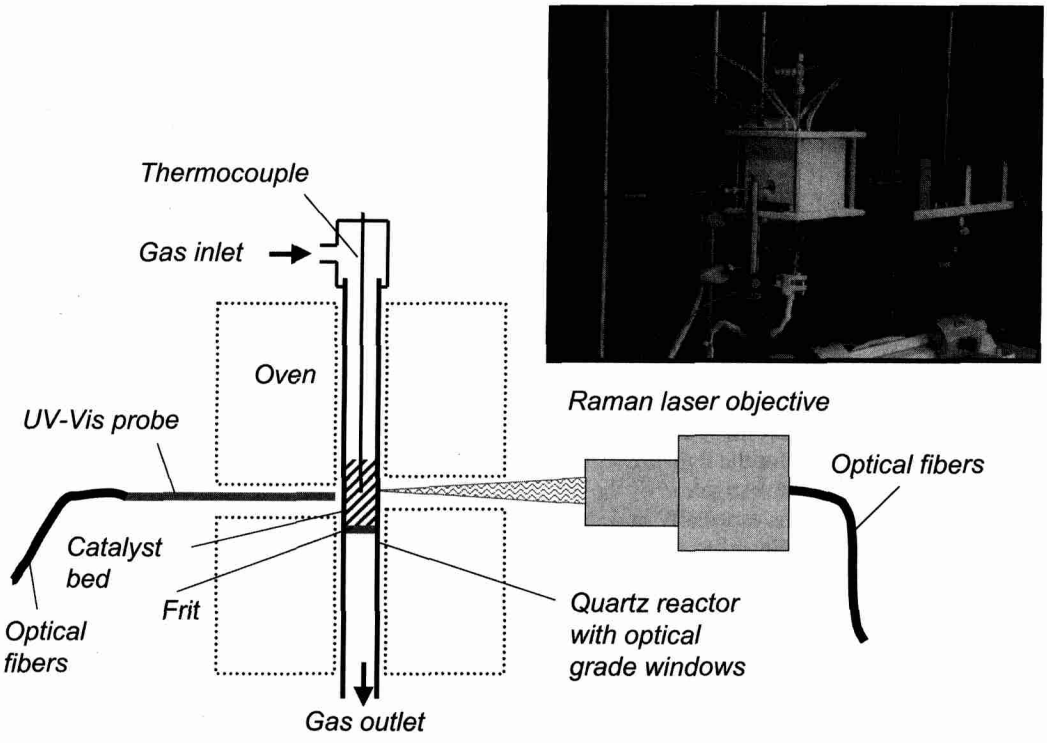

Figure 9. Scheme and picture of the combined *in-situ* DRS-Raman set-up for measuring catalytic solids operating in gas-phase reactions at elevated temperatures and ambient pressures.

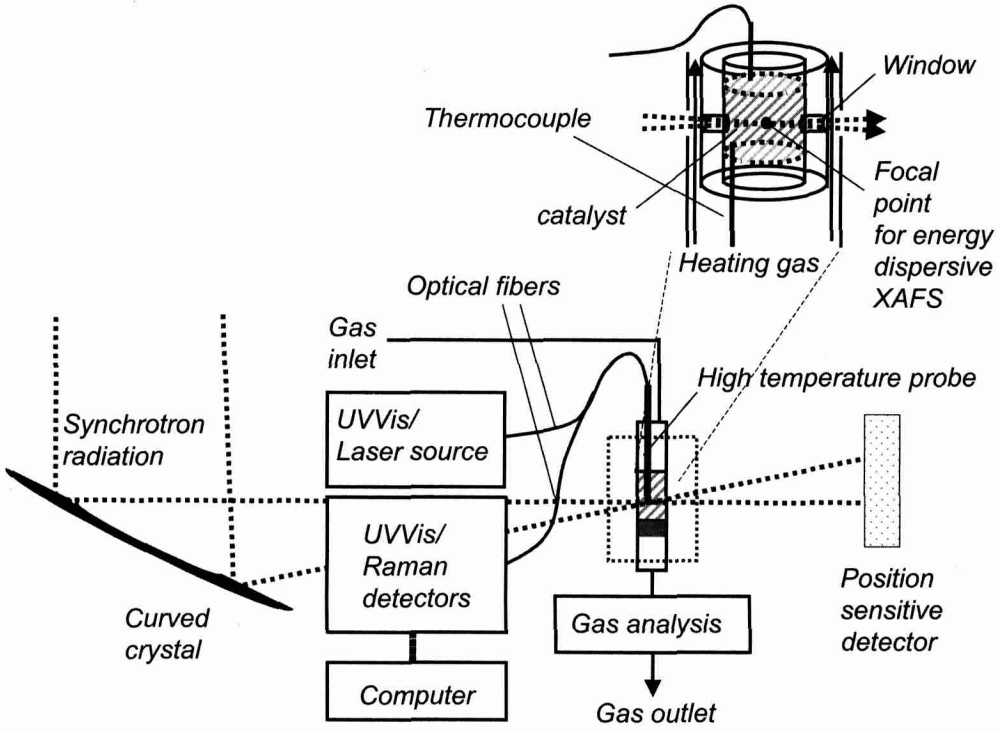

Figure 10. Scheme of an *in-situ* set-up for time-resolved measurements of catalytic solids making use of DRS, Raman and EXAFS spectroscopy. The set-up should allow the measurement of three sets of spectra in the second or sub-second region in one lab-scale reactor. Mass spectrometry or micro-gas chromatography will be used for on-line measuring of the catalytic performance. The envisaged set-up should be mobile since it has to be transferred to and installed at an appropriate EXAFS beamline.

reference materials (MgO, $BaSO_4$, Spectralon®, etc.) have reflectance losses at wavelengths below 250 nm. This leads to artefacts, which implies that recording spectra below 250 nm is not really reliable [14, 15]. In addition, reference materials must be stable toward water and other chemical compounds. The presence of contaminants may result in a decrease of the reflection in the NIR (e.g., water) and UV-VIS (e.g., (poly-)aromatics) region. Today, polytetrafluoroethylene (PTFE) is preferred over the more traditional reference materials (i.e., MgO and $BaSO_4$) because of its superior NIR performances [1, 2]. It is also important to notice that reference standards suffer from aging, and that they must be regularly checked, and, if necessary, replaced.

An alternative way of working is to use the bare oxide support (e.g., SiO_2, Al_2O_3, ZrO_2, TiO_2 and zeolites) as a reference material. In this manner, one can correct for the light absorption by the support, which may hamper the investigation of the absorption centers under study [1, 2]. This is especially important for supported transition metal ions with ligand-to-metal charge transfer transitions in the UV region (e.g., Re^{7+} and Ti^{4+}). Furthermore, when the catalyst support and supported metal oxide catalysts are studied in the same *in-situ* DRS cells, effects due to quartz windows of these DRS cells can be eliminated, provided that the scattering properties of the material are not changed by supporting the oxide material with transition metal ions. There are some indications that this is not always the case, especially in the UV region of the spectrum. As a rule of thumb, one should be aware that reliable quantitative *in-situ* DRS spectra of catalytic solids cannot be obtained below 250 nm.

Finally, it is important to mention some problems associated with the use of *in-situ* optical fiber probes. Such inserts in the reactor may interfere with the catalytic reaction under study. This gives rise to unselective reactions, leading to the formation of a layer of coke on top of the probe, gradually leading to spectra with decreasing signal-to-noise ratio. This can be circumvented by positioning the probe outside the reactor in close contact with an optical window of the reactor.

3. CASE STUDIES

3.1. Active Dehydrogenation Site and Structure-Activity Relationships for Cr/Al_2O_3 Catalysts

The annual growth rate of the demand for alkenes is currently very high. It is even expected to increase for propene in the next decade. This puts a lot of pressure on the operators of naphtha crackers. The catalytic dehydrogenation of alkanes is of great importance as an effective route for the direct production of light alkenes [33, 34]. A Cr/Al_2O_3 catalyst doped with an alkaline earth metal oxide (typical potassium) is industrially used for this process, and much research has been devoted to elucidate its active dehydrogenation site as well as its reaction and deactivation mechanism [35, 36]. The oxidation state of the active Cr-species for alkane dehydrogenation has been the subject of debate and controversy for many years. Both Cr^{3+} and Cr^{2+} have been proposed to be the active species.

The *in-situ* UV-Vis-NIR set-up outlined in Figure 7 has been used to develop quantitative structure-activity relationships for the dehydrogenation of isobutane over supported chromium oxide catalysts [24]. The method consists of four different steps. First, the number of required spectroscopic and catalytic experiments were optimized by using design of experiments (DOE). Five relevant experimental factors affecting the dehydrogenation process have been selected to mathematically describe the alkane dehydrogenation process. The factors are: (1) the SiO_2:Al_2O_3 ratio of a series of amorphous silica-alumina supports, expressed as the iso-electric point (IEP) (denoted as X_1 and expressed by a number between 2 (SiO_2) and 8 (Al_2O_3)); (2) the chromium oxide loading (denoted as X_2 and expressed in wt% Cr); (3) the gas composition (denoted as X_3 and expressed by the % isobutane diluted in nitrogen); (4) the reaction temperature (denoted as X_4 and expressed in °C); and, (5) the reaction time (denoted as X_5 and expressed in minutes). A five-level circumscribed central composite (CCC) DOE resulted in a set of 30 experiments.

Second, the dehydrogenation activity, expressed as response factor Y, was measured at the outlet of the *in-situ* DRS cell with on-line gas chromatography. This approach has already allowed the development of a quantitative relationship between the different Xs and Y:

$$Y^{1/2}(\%) = 2.284 - 0.195X_1 + 0.121X_2 - 0.132X_3 - 9.540.10^{-4}X_4 - 0.0610X_5 + 4.941.10^{-3}X_3^2 + 5.875.10^{-4}X_5^2 + 5.137.10^{-4}.X_1.X_4 - 4.480.10^{-3}X_2.X_3 + 8.008.10^{-4}X_3.X_5 \quad (8)$$

Eq. 8 allows the calculation of the conditions for maximum dehydrogenation activity over a series of supported chromium oxide catalysts based on $SiO_2.Al_2O_3$ supports. The following experimental conditions were obtained: $X_1 = 8$; $X_2 = 7.5$; $X_3 = 2$; $X_4 = 500$ and $X_5 = 10$. Thus, a maximum conversion is obtained after 10 minutes for a 7.5 wt% Cr/Al_2O_3 catalyst at 500°C with a mixture of 2% isobutane in nitrogen. In order to visualize Eq. 7, one can make conversion surface plots as illustrated in Figure 11. For example, Figure 11A predicts the catalytic activity after 30 minutes for a $Cr/SiO_2.Al_2O_3$ catalyst at 425°C as a function of the amount of isobutane in nitrogen and as a function of the chromium oxide loading. It is clear that the dehydrogenation activity gradually increases with increasing chromium oxide loading and decreasing amounts of isobutane in nitrogen. The influence of the reaction time and the chromium oxide loading on the predicted dehydrogenation activity of a $Cr/SiO_2.Al_2O_3$ catalyst at 425°C is illustrated in Figure 11B. It shows a gradual decrease in activity with increasing reaction time. The combined effect of the IEP of the support oxide and the reaction temperature on the catalytic activity is given in Figure 11C. One can notice that at high reaction temperatures, the dehydrogenation activity increases with increasing IEP; i.e., with an increasing amount of Al_2O_3 in the $SiO_2.Al_2O_3$ support.

In a third step, the speciation of chromium oxide species present under reaction conditions was measured by *in-situ* UV-Vis spectroscopy. An example of a set of spectra of a 0.5 wt% Cr/SiO_2 catalyst treated at 350°C in 2% isobutane is given in Figure 12. It shows a gradual decrease of absorption maxima around 360 and 450 nm with increasing reaction time at the expense of a new weak absorption band with a maximum at around 625 nm. The insert illustrates the presence of an isobestic point, suggesting the presence of at least two different

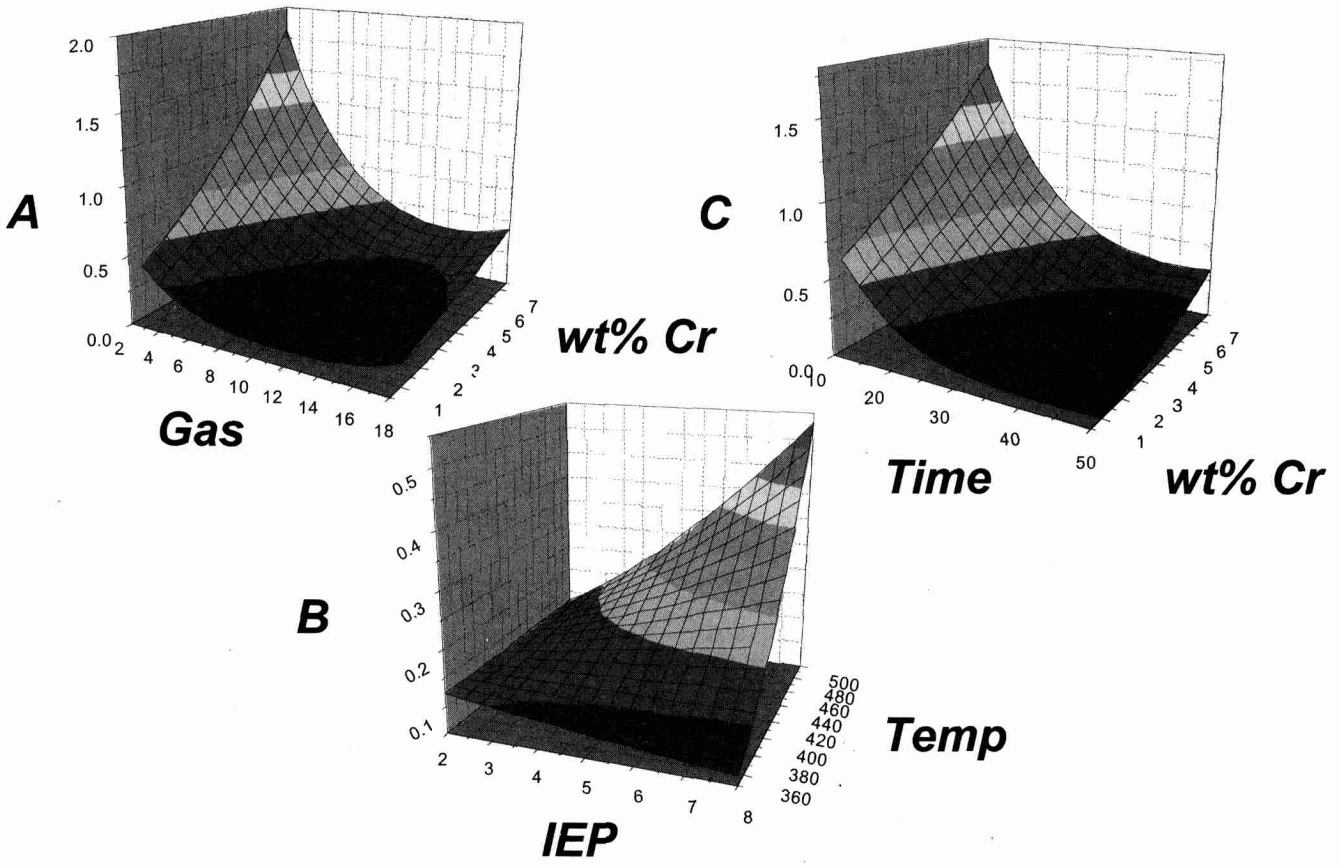

Figure 11. (A) Conversion surface plot of the gas composition and chromium oxide loading (the reaction temperature, isoelectric point of the support and the reaction time are set to 425°C, 5 and 10 minutes, respectively); (B) Conversion surface plot of the reaction time and chromium oxide loading (the isoelectric point, gas composition and reaction temperature are set to 5, 10% isobutane and 425°C, respectively); and, (C) Conversion surface plot of the isoelectric point of the support and the reaction temperature (the chromium oxide loading, gas composition and reaction time are set to 4 wt%, 10% isobutane and 30 minutes, respectively).

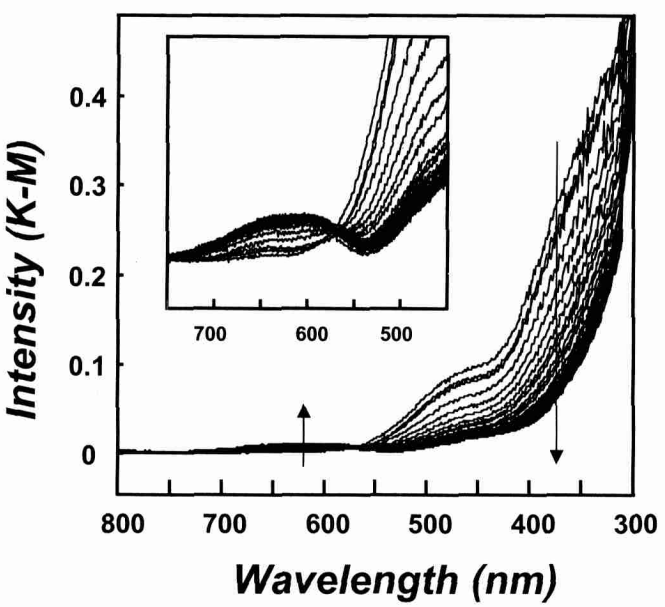

Figure 12. *In-situ* DRS spectra of 0.5 wt% Cr/SiO_2 catalyst treated at 350°C in 2% isobutane in N_2 as a function of time measured with the set-up of Figure 7.

chromium oxide species. The absorption bands located at 360 and 450 nm are the ligand-to-metal charge transfer (LMCT) transitions of Cr^{6+}, while the absorption band at 625 m is a d-d transition of reduced chromium oxide species ($Cr^{2+/3+}$) [35, 36]. The band intensity of the reduced chromium oxide species has been taken as a second response variable Z. One can now evaluate Z as a function of the five different experimental parameters Xs. This is illustrated in Figure 13 for the reaction temperature and the support composition, and it is clear that Z increases with increasing X_4 and X_1.

In a final step, a mathematical equation, which relates the dehydrogenation activity (response variable Y) with the amount of *in-situ* measured $Cr^{2+/3+}$ (response variable Z) was derived. Such a relationship can be envisaged as a quantitative structure-activity relationship, something which has been rarely developed in the field of catalysis. The mathematical equation for Cr/Al_2O_3 catalysts is illustrated in Figure 14. It can be concluded that the alkane dehydrogenation activity is directly proportional to the amount of reduced chromium oxide species formed under reaction conditions. The difference in catalytic activity between Cr/Al_2O_3 catalysts, which were 10 or 50 minutes on stream, must be explained in terms of coke deposited on the catalyst surface.

Although interesting information has been obtained with

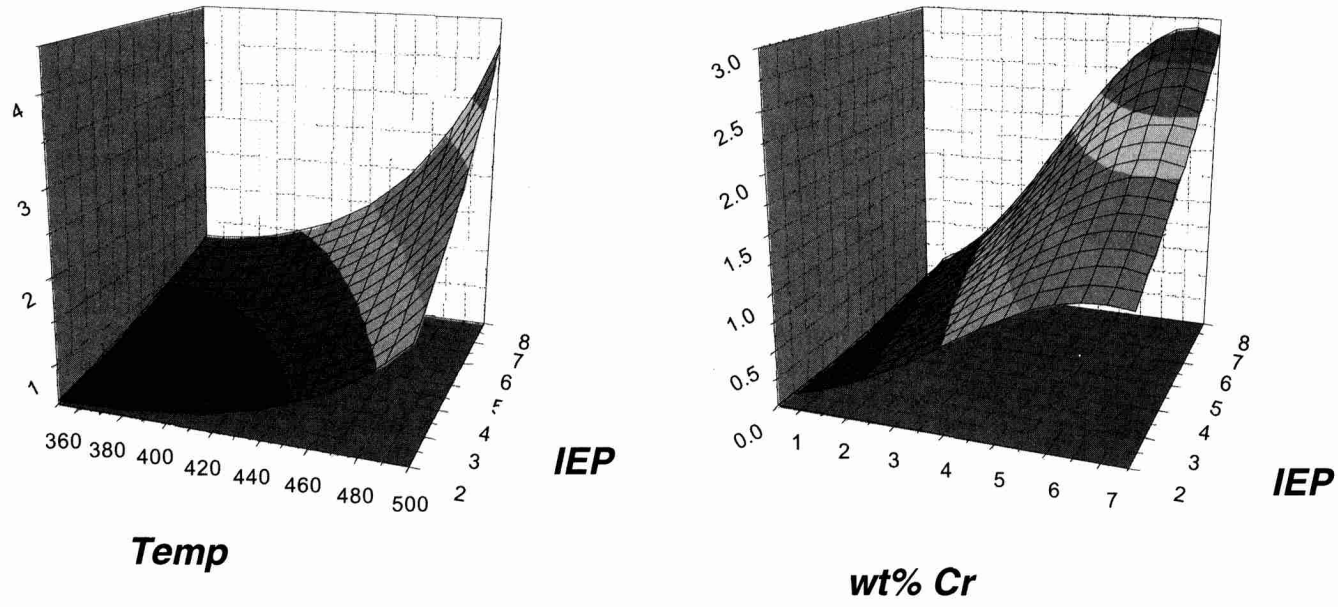

Figure 13. Reduced chromium oxide surface plot of the reaction temperature and the isoelectric point of the support (setting the chromium loading fixed to 7.5 wt%).

the *in-situ* DRS set-up of Figure 7, there are several problems associated with this equipment. First of all, the detection of diffuse reflected light was done with a PM leading to typical measurement times of about 1 min. Furthermore, the spectrum is collected wavelength after wavelength, which implies that the different parts of a spectrum do not represent the same reaction time. We also noticed an inaccurate temperature readout near the catalyst bed. Other disadvantages are that the temperature limit of the cell is close to 550°C and that the set-up hardly can be seen as a fixed-bed reactor. These problems were partially solved using an *in-situ* DRS set-up based on a high-temperature optical fiber probe positioned in a regular fixed-bed reactor (Figure 8) [26–28]. The time to measure a spectrum could be decreased to about 28 ms, but often 70 spectra had to be averaged to obtain a spectrum with a good signal-to-noise ratio. The use of a PDA or CCD detector allows the measurement of the whole spectral range at once and, as a consequence the different parts of a spectrum, represents the same reaction time. The temperature limitation for the high-temperature probe was still limited to about 600°C. Coke formation at the outer surface of the high-temperature probe also led to a lowering of the signal-to-noise ratio.

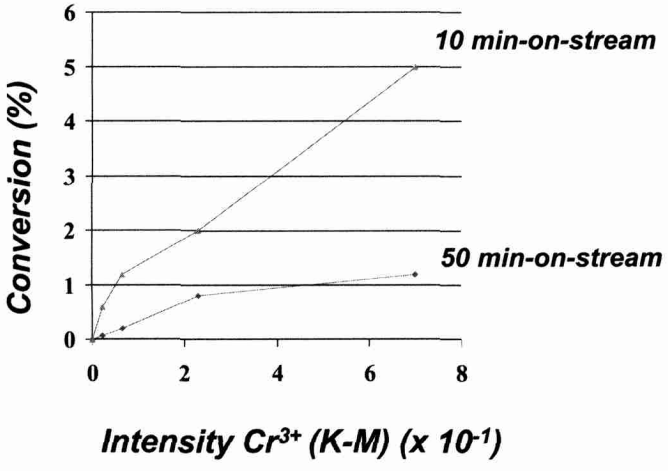

Figure 14. Quantitative relationship between the catalytic activity (response Y) and the amount of reduced Cr (response Z) as predicted for 10 and 50 minutes on stream.

However, in our latest *in-situ* DRS set-up (Figure 9) [31, 32], we are able (1) to use probes operating at temperatures as high as 800°C, (2) to measure spectra in the range of 200–1100 nm, enabling us to measure a small part of the NIR region, (3) to decrease the measurement time of one spectrum down to 6 ms, and (4) to improve the signal-to-noise ratio with a better detector. The Raman spectra can be recorded with a typical time resolution of about 1 min.

Figures 14–16 illustrate the potential of the combined DRS-Raman set-up for studying the alkane dehydrogenation site of a 0.5 wt% Cr/Al_2O_3 catalyst. UV-Vis-NIR, Raman and catalytic data were simultaneously measured during four successive dehydrogenation-regeneration cycles at 580°C. Figure 15 shows the measured catalytic activity data for the dehydrogenation of propane to propene as measured with micro-gas chromatography. It can be seen that the catalyst performance does not change from one dehydrogenation cycle to the next one, but changes significantly within one dehydrogenation cycle. The conversion of propane to propene gradually increases with increasing time-on-stream and reaches a maximum of 10% at the end of the dehydrogenation cycle, which is after 28 min. Longer reaction times do not significantly increase the yield of propene. This can be seen in the 4th dehydrogenation cycle, which takes more than 1 h. Thus, a stable dehydrogenation activity of about 10% could be obtained and maintained over this catalyst for more than 1 h and for successive dehydrogenation-regeneration cycles.

As an example, Figure 16 illustrates the changes taking

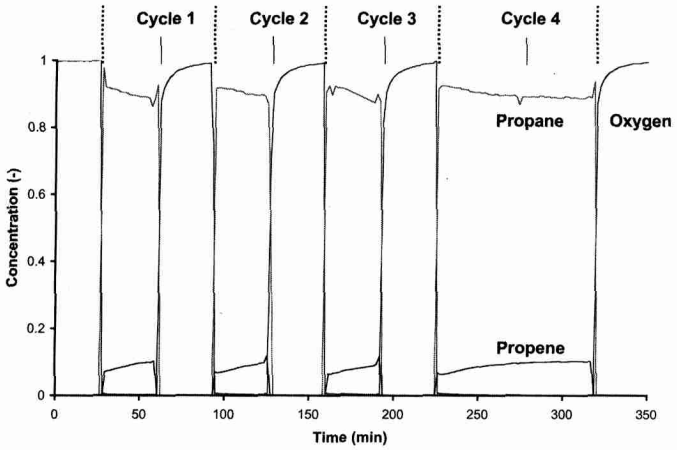

Figure 15. Conversion of propane to propene at 580°C over a 0.5 wt% Cr/Al_2O_3 catalyst during four successive dehydrogenation-regeneration cycles.

place in the UV-Vis-NIR spectra for the first dehydrogenation cycle as a function of time. The initial spectrum of the Cr/Al_2O_3 catalyst treated in oxygen is characterized by the two intense LMCT transitions of Cr^{6+} at 270 and 380 nm [35, 36]. These bands gradually decrease in intensity within the first 15 s of the dehydrogenation cycle and this intensity decrease is accompanied by the formation of CO_2. Thus, Cr^{6+} is reduced to a lower oxidation state in the presence of propane. The presence of an isobestic point at around 582 nm confirms this gradual transformation of Cr^{6+} to reduced chromium oxide species. This second surface Cr-species is characterized by absorption bands located at 465 and 650 nm, which are typical d-d transitions of pseudo-octahedral Cr^{3+} [35, 36]. No indication of Cr^{2+}-species could be observed in the UV-Vis-NIR spectra at lower energy values. With our two previous set-ups (Table 1), the measured UV-Vis spectra did not extend to sufficiently low energy to exclude the presence of pseudo-tetrahedral Cr^{2+}. Thus, by measuring down to 1100 nm in the NIR region, we can state that Cr^{3+}-sites are exclusively formed under typical propane dehydrogenation conditions. This observation allows us to conclude that Cr^{3+}-species are the active alkane dehydrogenation sites. The sharp negative peaks located at 532 and 1064 nm are due to interference by light of the Raman laser scattered at the catalyst particles, while the spike at 656 nm is an artifact of the UV-Vis-NIR spectrometer.

In the oxidation cycles, the coke formed during alkane dehydrogenation is combusted from the catalyst as can be concluded from the formation of CO_2 in the beginning of the regeneration cycles, from the increase of the catalyst bed temperature and the decrease of the Raman bands in the 1200–1650 cm^{-1} region. During the catalyst regeneration, the *in-situ* UV-Vis-NIR spectra return completely to the initial state (Figure 16), but the re-oxidation of Cr^{3+} to Cr^{6+} with oxygen is much slower than the reduction of surface chromate in propane during the dehydrogenation cycle (Figure 15). Indeed, it takes about 1 min before the Cr^{6+} LMCT-bands at 270 and 280 nm are gaining their initial intensities during catalyst regeneration. This suggests that the active Cr^{3+}-sites are somehow buried by coke or are partially diffus-

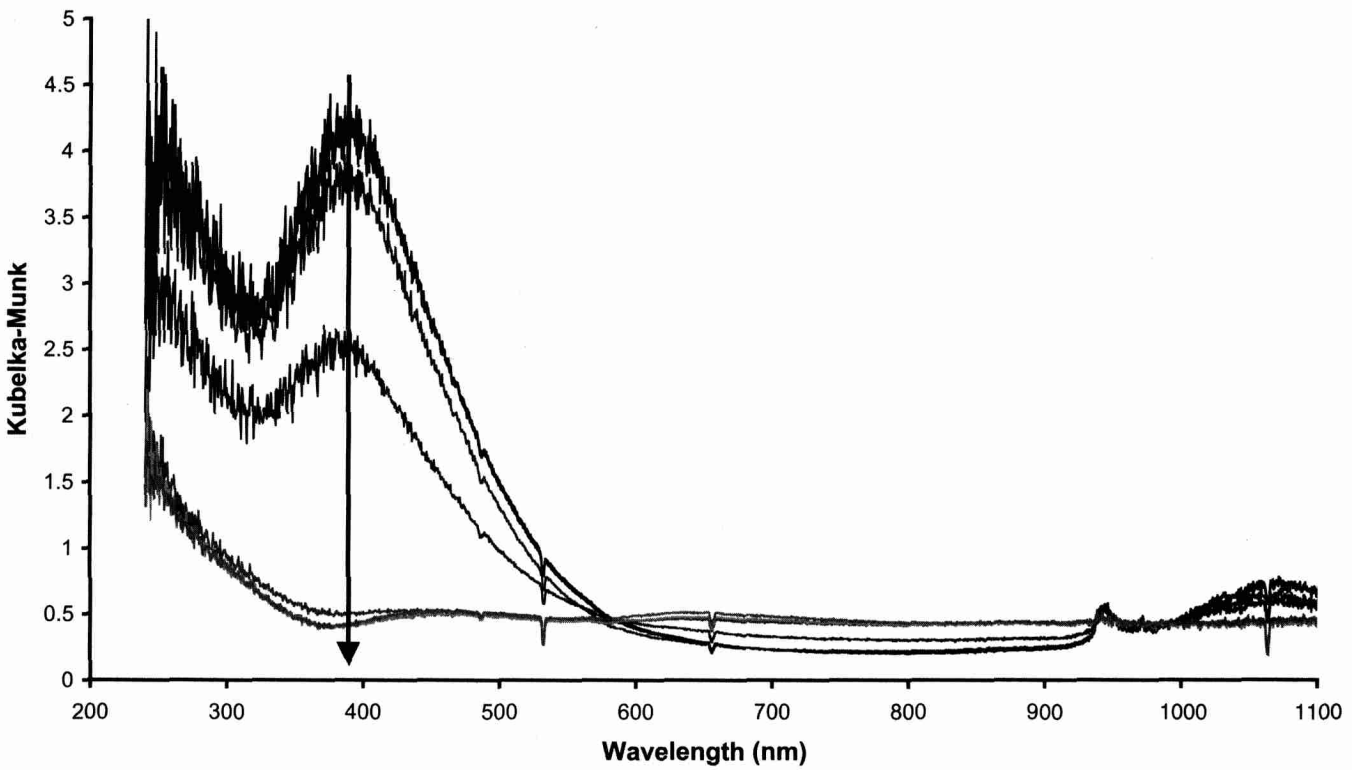

Figure 16. *In-situ* UV-Vis-NIR spectra of a 0.5 wt% Cr/Al_2O_3 catalyst measured during the 1st dehydrogenation cycle in a stream of propane in He at 580°C as a function of time on stream.

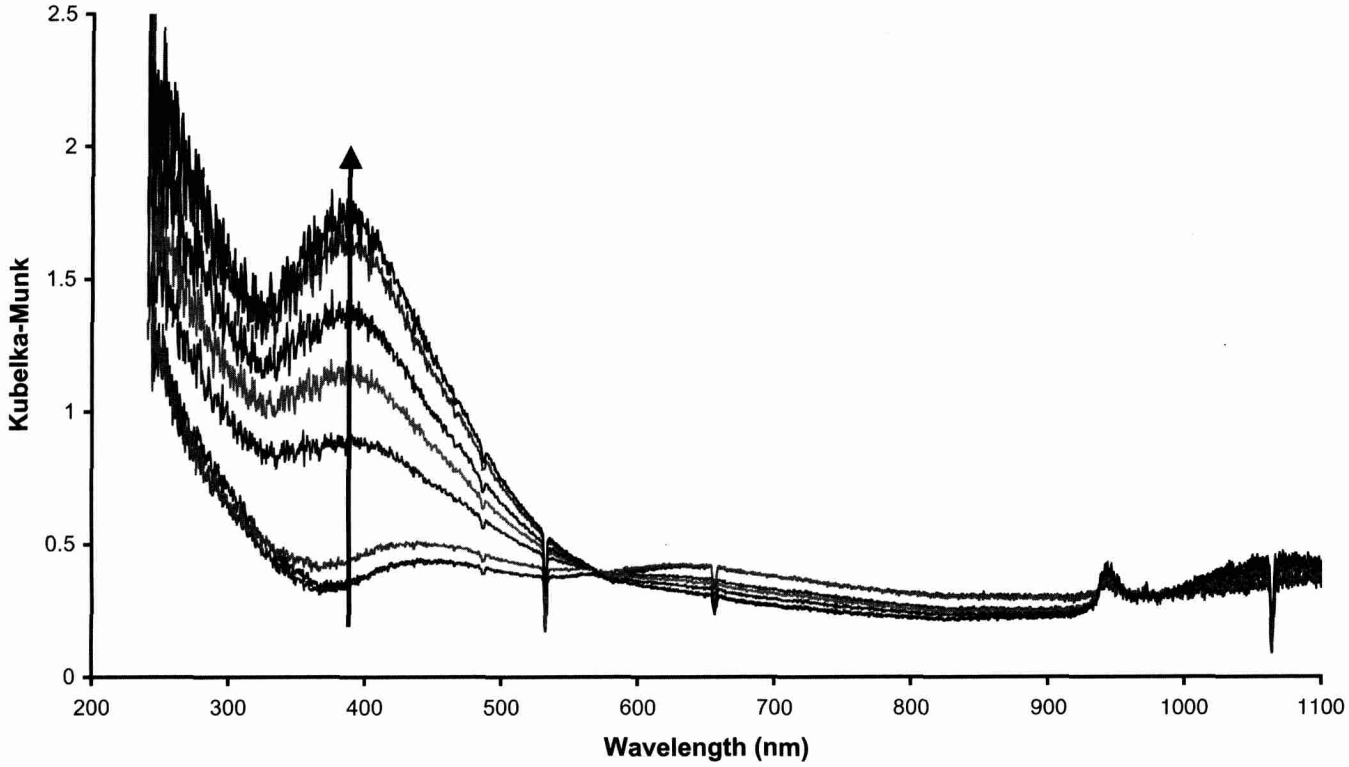

Figure 17. *In-situ* UV-Vis-NIR spectra of a 0.5 wt% Cr/Al_2O_3 catalyst measured during the 1st regeneration cycle in a stream of oxygen at 580°C as a function of time on stream.

ing into the alumina support surface, hampering their fast re-oxidation. Summarizing, pseudo-octahedral Cr^{3+}-sites are formed under typical alkane dehydrogenation conditions. These surface species can be proposed as the active sites for this catalytic process since no pseudo-octahedral and pseudo-tetrahedral Cr^{2+}-species could be observed under reaction conditions.

3.2. Physicochemical Processes During the Hydrothermal Crystallization of Microporous CoAPO-5 Molecular Sieves

Zeolites are an important group of molecular sieves, which are heavily used as heterogeneous catalysts in petrochemical industries. One of the greatest challenges is to understand the physicochemical principles that determine how microporous crystalline solids are formed under hydrothermal conditions [37]. This is not easy because hydrothermal crystallizations are chemical reactions, in which many interactions and equilibria continuously change with crystallization time [38]. The lack of knowledge about these systems means that a rational design of novel zeolites is still impossible. An attractive, but almost unexplored way of probing the hydrothermal crystallization process is to do *in-situ* characterization studies in real time and under realistic laboratory conditions; i.e., at high temperatures (e.g., 200°C) and pressures (e.g., 15 bar).

Recently, we have developed a method based on *in-situ* diffuse reflectance spectroscopy in the UV-Vis-NIR region for probing the changes in the coordination environment of transition metal ions during the hydrothermal crystallization of microporous aluminophosphates [13]. Figure 18 illustrates the structure and composition of the most important member of the family of microporous aluminophosphates, namely $AlPO_4$-5. This material is obtained by the condensation of tetrahedra of Al^{3+} and P^{5+}, giving a three-dimensional network with one-dimensional channels of a diameter of about 0.74 nm. Al^{3+} and P^{5+} can be replaced by transition metal ions, such as Co^{2+}, Ni^{2+}, Cr^{3+} and V^{4+}. One question is if

Table 1. Comparison of the performances and requirements of different set-ups for measuring *in-situ* UV-VIS-NIR spectra.

Performances and requirements	Praying Mantis UV-Vis set-up	Fiber optic UV-Vis set-up	Combined DRS-Raman set-up
Time needed to acquire a UV-Vis spectrum	60 s	0.028 s	0.006 s
Spectral range of UV-Vis spectrum	200–800 nm	200–800 nm	200–1100 nm
Different parts of the UV-Vis spectrum represent the same time	No	Yes	Yes
Temperature limitation of UV-Vis probe	550°C	600°C	800°C
Reactor requirements	Optical cell	Fixed-bed reactor	Fixed-bed reactor

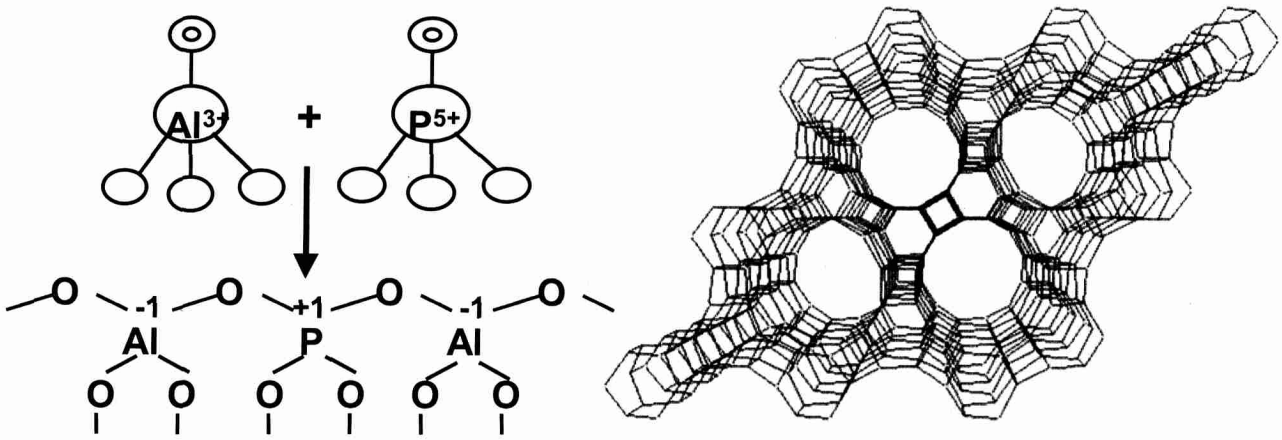

Figure 18. Schematical representation of $AlPO_4$-5 molecular sieves. The three-dimensional network is made by condensation of oxygen tetrahedra of Al^{3+} and P^{5+}.

these transition metal ions really incorporate in the framework of these molecular sieves. *In-situ* DRS spectroscopy may be helpful in answering this fundamental question. This has been done by using the *in-situ* DRS cell schematically illustrated in Figure 6. The cell has been placed in front of a regular DRS spectrophotometer, allowing the measurement of spectra in the range 200–2500 nm.

The *in-situ* DRS spectra obtained during hydrothermal crystallization are characterized by d-d transitions characteristic for the specific transition metal ion, as well as by the overtone and combination bands of the fundamental vibrations of water and template molecules present in the synthesis gel. An overall observation is that the overtone and combination bands gradually decrease in intensity with increasing synthesis time, while the intensities of the d-d transitions of the transition metal ions gradually increase during the course of the synthesis process. Table 2 gives an overview of the d-d absorption bands observed in the DRS spectra of the CoAPO-5, CrAPO-5, NiAPO-5 and VAPO-5 gel materials at room temperature, at 175°C and after 24 h of the hydrothermal synthesis at 175°C; and the corresponding color changes.

Figure 19 shows the *in-situ* DRS spectra of the CoAPO-5 gel as a function of the synthesis time. The spectrum of the initially pink-colored CoAPO-5 gel is characterized by absorption bands at 521 and 470 nm. An isobestic point is clearly visible after gradually heating the synthesis gel to 175°C. The absorption band at 521 nm can be assigned to the d-d transition of octahedral Co^{2+}, while the band at 470 nm is indicative for the presence of a second type of octahedral Co^{2+}, most probably a $CoO_4(H_2O)_2$ species. Further heating of the synthesis gel results in a gradual change of the color from pink to light-blue, and a triplet with absorptions at 542, 584 and 625 nm is observed in the DRS spectrum. This triplet, which is assigned to the d-d transition of tetrahedral Co^{2+}, strongly increases in intensity with increasing synthesis time and becomes the most intense after 24 h. A very intense blue colored and highly crystalline CoAPO-5 material was obtained. It is important to notice that X-ray diffraction (XRD) indicates that no crystalline phase was formed during the first hours of the synthesis process, whereas synthesis times higher than 24 h lead to the formation of less crystalline or even other crystalline phases, such as CoAPO-C. Thus, *in-situ* DRS together with XRD indicate the gradual formation of CoAPO-5 molecular sieves and a transformation of an octahedral (gel-type) Co^{2+}-species to a pseudo-tetrahedral (framework-type) Co^{2+}-species. In addition, a pseudo-octahedral $CoO_4(H_2O)_2$-species is observed in the initial stages of the synthesis process.

The evolution of the *in-situ* DRS spectra of the CrAPO-5 materials as a function of the synthesis time is shown in Figure 20. They are completely different from those obtained for CoAPO-5 molecular sieves. The DRS spectrum of the initial blue-grey colored CrAPO-5 gel is characterized by absorption bands at 583, 415 and 300 nm, which can be as-

Table 2. Overview of the d-d absorption bands (in nm) observed in the *in-situ* DRS spectra of CoAPO-5, CrAPO-5, NiAPO-5 and VAPO-5 gel materials at room temperature, at 175°C and after 24 h of hydrothermal synthesis at 175°C. The corresponding color changes are also included (with sh = shoulder).

Material	Synthesis gel at room temperature	Synthesis gel heated up to 175°C	After 24 h of synthesis at 175°C
CoAPO-5	470 (sh); 527	542; 584; 625	542; 584; 625
	pink	*light blue*	*dark blue*
CrAPO-5	300; 415; 583	300; 445; 625	300; 445; 625
	blue-gray	green	green
NiAPO-5	399; 460 (sh); 668 (sh); 739	400 (sh); 684 (sh); 761	408; 688; 763
	light green	*light green*	*white green*
VAPO-5	400 (sh); 630; 850	400 (sh); 630; 850	625; 850
	light green	*light green*	*light green*

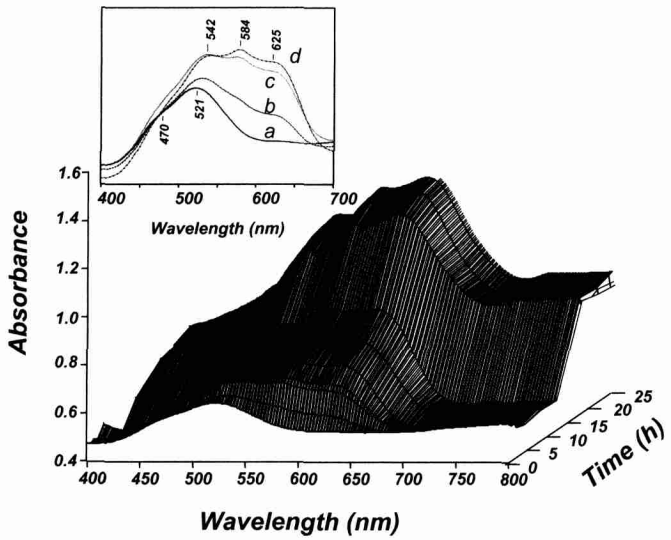

Figure 19. *In-situ* DRS spectra of the CoAPO-5 gel as a function of the synthesis time. The insert shows some DRS spectra as a function of the heating temperature in the initial stages of the hydrothermal synthesis: (a) room temperature; (b) 60°C; (c) 100°C; and, (d) 175°C.

signed to the three d-d transitions of octahedral Cr^{3+}. Heating the gel to 60°C results in a drastic change of the color from blue-grey to green, and the absorption bands in DRS are red-shifted to 625 nm and 445 nm. This shift indicates small changes in the octahedral coordination environment of Cr^{3+}. Further heating of the gel to 175°C did not significantly alter the *in-situ* DRS spectra. Continuing the synthesis at 175°C resulted in similar DRS spectra and a green-colored highly crystalline CrAPO-5 material was obtained. Here again, no crystalline phase was formed during the first hours of the synthesis process, whereas synthesis times higher than 24 h lead

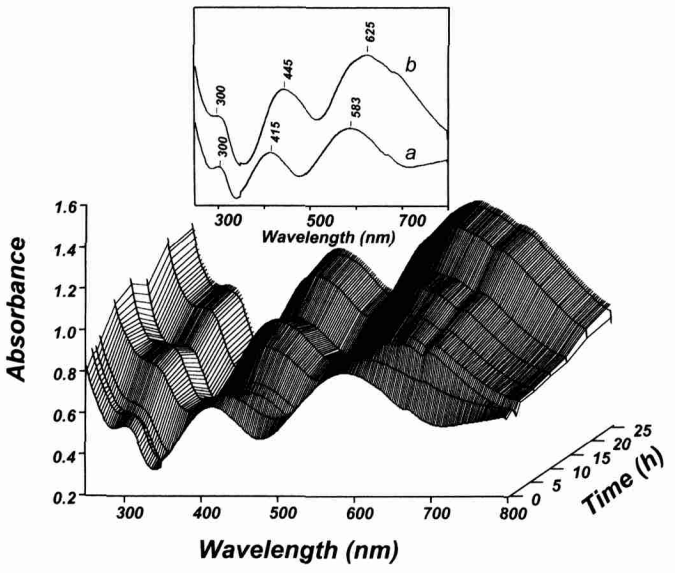

Figure 20. *In-situ* DRS spectra of the CrAPO-5 gel as a function of the synthesis time. The insert shows some DRS spectra as a function of the heating temperature in the initial stages of the hydrothermal synthesis: (a) room temperature; and, (b) 60°C.

to the formation of less crystalline or even other crystalline phases. Thus, *in-situ* DRS spectroscopy indicates the formation of pseudo-octahedral Cr^{3+}-species in the gel material and no transformation of Cr^{3+} take place in the heating process of the gel up to 60°C and not during the real crystallization process of CrAPO-5 molecular sieves at 175°C.

The DRS spectrum of the initial synthesis gel of NiAPO-5 is characterized by a relatively intense absorption band at 399 nm with a weak shoulder at around 460 nm. In addition, two broad absorption bands at 668 and 739 nm are visible. Heating the synthesis gel up to 175°C resulted in a small red-shift of the absorption band at 399 to 406 nm and a disappearance of the shoulder at 460 nm. The white-green colored highly crystalline NiAPO-5 material recovered from the DRS cell after synthesis for 24 h is characterized by absorption bands at 408, 688 and 763 nm. These three absorption bands are the characteristic d-d transitions of pseudo-octahedral Ni^{2+}. XRD revealed no crystalline phases in the initial stage of the synthesis process and during the heating process.

The *in-situ* DRS spectrum of a fresh light-green VAPO-5 synthesis gel is characterized by d-d absorption bands at 630 and 850 nm and one shoulder at around 400 nm. This shoulder gradually disappears with increasing heating temperature of the gel and becomes very weak in the DRS spectrum of the synthesis gel at 175°C. The shoulder completely disappears after heating the synthesis gel for 24 h, although the main absorption bands at 630 and 850 nm remain visible and even intensify. These two absorption bands are the d-d transitions characteristic of pseudo-octahedral $V{=}O^{2+}$-species. Again no crystalline phase was formed during the first hours of the synthesis process.

Based on these *in-situ* DRS observations we may conclude that there is no clear evidence for the isomorphous substitution of V^{4+}, Cr^{3+} and Ni^{2+} in the framework of $AlPO_4$-5 molecular sieves. These transition metal ions are always present in the initial gel, the heated gel and the final crystalline MeAPO-5 material as pseudo-octahedral ions. The most pronounced spectral changes even take place during the initial heating process of the gel material. At this stage of the synthesis, we did not observe any crystalline MeAPO-5 material with XRD. Only in the case of CoAPO-5 materials have we found clear evidence for the formation of pseudo-tetrahedral Co^{2+} in a framework position. Furthermore, we were able to observe a special Co^{2+}-species, which we consider as an intermediate in the isomorphous substitution process.

3.3. Reaction Mechanism for the NO Decomposition Over Cu-ZSM-5 Zeolites

A very attractive method for the removal of NO is its direct decomposition into molecular N_2 and O_2 [39]. Although the decomposition of NO is thermodynamically favored at temperatures below 700°C, the reaction is kinetically retarded due to the very high activation energy. A whole series of catalysts was explored over the last few decades and Iwamoto et al. have reported the high and stable activity of over-exchanged Cu-ZSM-5 catalysts for the direct decomposition of NO [40]. Quite a lot of research has been devoted to the identification of the active sites in Cu-ZSM-5 and the related NO decomposition reaction mechanism.

The proposed reaction mechanism for the decomposition

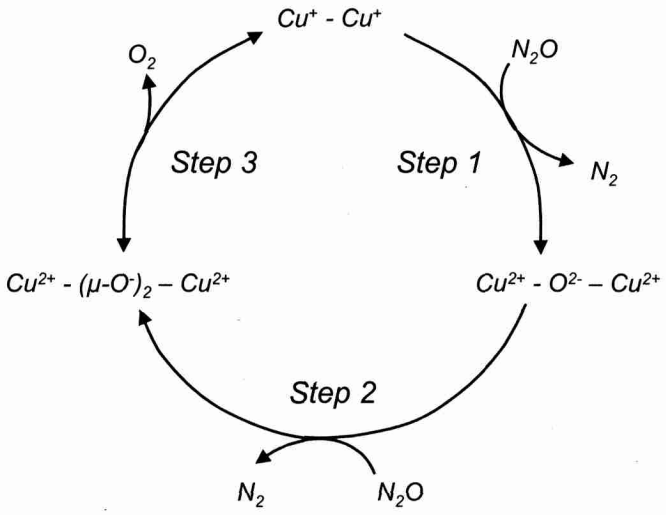

Figure 21. Reaction scheme for the decomposition of N_2O over Cu-ZSM-5 catalysts. The roles of two key reaction intermediates are illustrated.

of N_2O over Cu-ZSM-5 zeolites is shown in Figure 21 [41]. The scheme is considered to be very similar to that for the decomposition of NO. The cycle starts from a $Cu^{+}\cdots Cu^{+}$ pair, which reacts with N_2O forming a Cu^{2+}-O^{2-}-Cu^{2+} species and N_2. Further reaction with N_2O results in the formation of a $[Cu_2(\mu\text{-}O)_2]^{2+}$ complex, which releases in a third step O_2 with the reformation of the $Cu^{+}\cdots Cu^{+}$. *In-situ* UV-Vis-NIR spectroscopy has been used to elucidate this reaction mechanism and evidence for the formation of two reaction intermediates; i.e., the Cu^{2+}-O^{2-}-Cu^{2+} species (with an absorption band at 740 nm) and the $[Cu_2(\mu\text{-}O)_2]^{2+}$ species (with an absorption band at 465 nm) [41, 42].

Figure 22 shows the changes in the *in-situ* DRS spectra of Cu-ZSM-5 in the presence of N_2O for increasing reaction temperature. One can notice that the absorption band at 740 nm decreases at the expense of the absorption band at 465 nm for increasing reaction temperature. This implies that

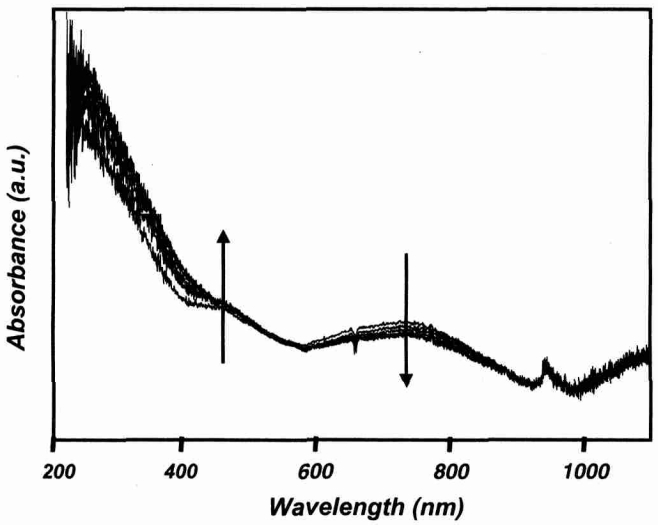

Figure 22. *In-situ* DRS spectra of Cu-ZSM-5 in the presence of N_2O for increasing reaction temperature (temperature range = 280–470°C).

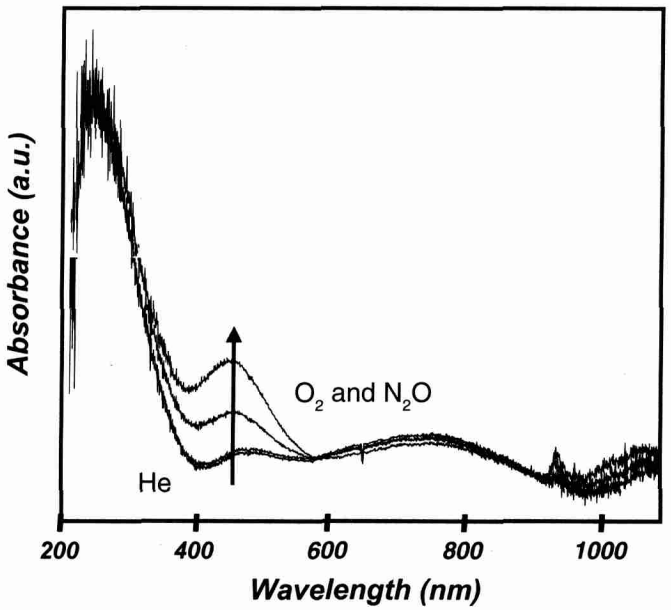

Figure 23. *In-situ* DRS spectra of Cu-ZSM-5 in the presence and absence of O_2 or N_2O at 470°C.

the bis-μ-oxo copper species is more stable at high reaction temperature than at low reaction temperature. Because a reaction intermediate will be observed in the *in-situ* spectra when it is participating in the rate-determining step, we assume that at high reaction temperatures the rate-determining step is step three in which oxygen is released from the bis-μ-oxo copper species. The bis-μ-oxo copper species disappears at 450°C when the N_2O stream is changed for a He stream (Figure 23). The band readily reappears when O_2 or N_2O is again added to the reaction mixture. In the case of O_2, the intensity is even much more pronounced. These phenomena can be explained by the removal of O_2 from the bis-μ-oxo copper complex when He is present and consequently the $Cu^{+}\cdots Cu^{+}$-species is formed. Addition of O_2 can regenerate the bis-μ-oxo copper complex. This implies that step 3 is a reversible step. O_2 adsorption seems to be a very fast step since the bis-μ-oxo

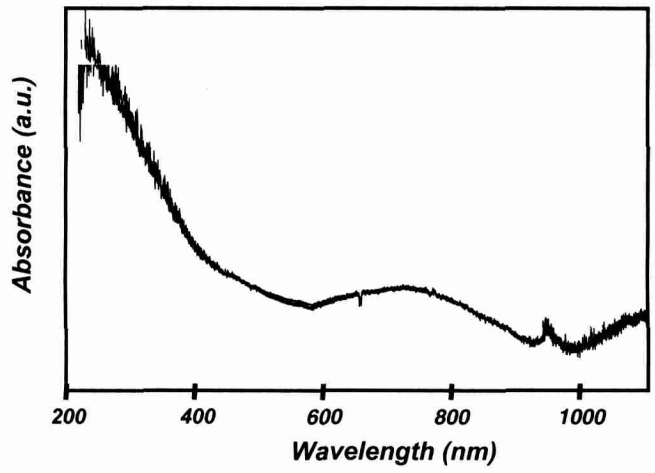

Figure 24. *In-situ* DRS spectra of Cu-ZSM-5 in the presence and absence of O_2 (a) or N_2O (b) at 280°C.

copper species can be regenerated already after 2 minutes, whereas its disappearance requires about 30 minutes. In the case of the addition of N_2O, the bis-μ-oxo copper species is generated by the consecutive steps 2 and 3. Also this process is relatively fast compared to its disappearance in the presence of He (2 vs. 15 minutes). The situation is totally different at a reaction temperature of 280°C. This is illustrated in Figure 24. Changing the gas composition from N_2O to He, or later to O_2 and back to N_2O over a Cu-ZSM-5 catalysts, did not alter the *in-situ* DRS spectra. In all cases, the absorption band of the Cu^{2+}-O^{2-}-Cu^{2+} species at 740 nm is dominant. This implies that step 2 in the reaction mechanism shown in Figure 21 is rate-determining at low reaction temperatures.

4. CONCLUDING REMARKS

Diffuse reflectance spectroscopy in the ultraviolet, visible and near-infrared region is a versatile spectroscopic technique to probe the coordination environment and oxidation state of transition metal ions in catalytic solids under reaction conditions. Several *in-situ* devices are available, making the technique very useful for detailed mechanistic investigations and the identification of active sites and reaction intermediates. Such information is necessary if one wants to develop quantitative structure-activity relationships in the field of catalysis. Unfortunately, such an approach is still in its infancy, although DRS is one of the few techniques that allows the measurement of *in-situ* spectra in a quantitative manner. Only by a systematic and intelligent application of the *in-situ* DRS technique, in conjunction with mathematical and statistical routines, can all of the necessary information be extracted and fully appreciated. This will be necessary if we want to use *in-situ* spectroscopy as a tool for the rational design of new catalysts.

ACKNOWLEDGMENTS

B. M. W. acknowledges the Dutch Science Foundation (NWO-CW) for a Van der Leeuw and VICI grant. The author is grateful to the following persons for their contributions to the work covered in case study 1 (A. A. Verberckmoes, J. Debaere, R. L. Puurunen, B. G. Beheydt, A. Mens, T. A. Nijhuis and S. J. Tinnemans), case study 2 (D. Baetens and H. Leeman) and case study 3 (M. G. Groothaert, K. Lievens, H. Leeman and T. A. Nijhuis). B. M. W. also acknowledges R. A. Schoonheydt for the many fruitful discussions on *in-situ* diffuse reflectance spectroscopy.

REFERENCES

1. Weckhuysen, B. M., in *Spectroscopy of transition metal ions on surfaces*, Weckhuysen, B. M., Van Der Voort, P., Catana, G., (Eds.), Leuven University Press, (2000), p. 221.
2. Weckhuysen, B. M., Schoonheydt, R. A., *Catal. Today*, 49, 441 (1999).
3. Melsheimer, J., Ziegler, D., *J. Chem. Soc. Faraday Trans. I*, 83, 1109 (1987).
4. Forster, H., Seebode, J., Fejes, P., Kiricsi, I., *J. Chem. Soc. Faraday Trans. I*, 83, 1109 (1987).
5. Forster, H., Franke, S., Seebode, J., *J. Chem. Soc. Faraday Trans. I*, 39, 357 (1983).
6. Sendoda, Y., Ono, Y., Keii, T., *J. Catal.*, 39, 357 (1975).
7. Kortüm, G., *Reflectance spectroscopy*, Springer-Verlag, Berlin, (1969).
8. Schoonheydt, R. A., in *Characterization of Catalysts*, F. Delannay (Ed.), Marcel Dekker, (1984), p. 125.
9. Kellerman, R., in *Spectroscopy in Heterogeneous Catalysis*, Delgass, W. N., Haller, G. L., Kellerman, R., Lunsford, J. H., (Eds.), Academic Press, New York, (1979), p. 86.
10. Klier, K., in *Vibrational Spectroscopies for Adsorbed Species*, Bell, A. T., Hair, M. L., (Eds.), ACS Symp. Ser. 137, 141 (1980).
11. Schoonheydt, R. A., in *Advanced Methods in Clay Minerals Analysis*, Fripiat, J. J., (Ed.), Elsevier, Amsterdam, (1981), p. 169.
12. Klier, K., *J. Opt. Soc. Am.*, 62, 882 (1972).
13. Weckhuysen, B. M., Baetens, D., Schoonheydt, R. A., *Angew. Chem. Int. Ed.*, 39, 3419 (2000).
14. Ahmad, R., Melsheimer, J., Jentoft, F. C., Schlogl, R., *J. Catal.*, 218, 365 (2003).
15. Melsheimer, J., Thiede, M., Ahmad, R., Tzolova-Muller, G., Jentoft, F. C., *Phys. Chem. Chem. Phys.*, 5, 4366 (2003).
16. Optical Spectroscopy: Sampling Techniques Manual. Harric Scientific Corporation, New York, (1987).
17. Gao, X., Jehng, J. M., Wachs, I. E., *J. Catal.*, 209, 43 (2002).
18. Gao, X., Banares, M. A., Wachs, I. E., *J. Catal.*, 188, 325 (1999).
19. Gao, X., Bare, S. R., Weckhuysen, B. M., Wachs, I. E., *J. Catal.*, 188, 325 (1999).
20. Chen, K. D., Bell, A. T., Iglesia, E., *J. Phys. Chem. B*, 104, 1292 (2000).
21. Chen, K. D., Iglesia, E., Bell, A. T., *J. Catal.*, 192, 197 (2001).
22. Argyle, M. D., Chen, K. D., Resini, C., Krebs, C., Bell, A. T., Iglesia, E., *Chem. Commun.*, 2082 (2003).
23. Weckhuysen, B. M., Bensalem, A., Schoonheydt, R. A., *J. Chem. Soc. Faraday Trans.*, 94, 2011 (1998).
24. Weckhuysen, B. M., Verberckmoes, A. A., Debaere, J., Ooms, K., Langhans, I., Schoonheydt, R. A., *J. Mol. Catal. A: Chemical*, 151, 115 (2000).
25. Bensalem, A., Weckhuysen, B. M., Schoonheydt, R. A., *J. Phys. Chem. B*, 101, 2834 (1997).
26. Puurunen, R. L., Beheydt, B. G., Weckhuysen, B. M., *J. Catal.*, 204, 253 (2001).
27. Puurunen, R. L., Weckhuysen, B. M., *J. Catal.*, 210, 418 (2002).
28. Weckhuysen, B. M., *Chem. Commun.*, 97 (2002).
29. Bruckner, A., *Catal. Rev. Sci. Eng.*, 45, 97 (2003).
30. Bruckner, A., *Chem. Commun.*, 2122 (2001).
31. Nijhuis, T. A., Tinnemans, S. J., Visser, T., Weckhuysen, B. M., *Phys. Chem. Chem. Phys.*, 5, 4361 (2003).
32. Weckhuysen, B. M., *Phys. Chem. Chem. Phys.*, 5, 4351 (2003).
33. Sanfilippo, D., *Cattech*, 4, 56 (2000).
34. Bhasin, M. M., McCain, J. H., Vora, B. V., Imai, T., Pujado, P. R., *Appl. Catal. A General*, 221, 397 (2001).
35. Weckhuysen, B. M., Schoonheydt, R. A., *Catal. Today*, 51, 223 (1999).
36. Weckhuysen, B. M., Wachs, I. E., Schoonheydt, R. A., *Chem. Rev.*, 96, 3327 (1996).
37. Lok, B. M., Cannon, T. R., Messina, C. A., *Zeolites*, 3, 282 (1983).
38. Davis, M. E., Lobo, R. F., *Chem. Mater.*, 4, 756 (1992).
39. Shelef, M., *Chem. Rev.*, 95, 209 (1995).
40. Iwamoto, M., Furukawa, H., Mine, Y., Uemura, F., Mikuriya, S. I., Kagawa, S., *J. Chem. Soc. Chem. Commun.*, 1272 (1986).
41. Groothaert, M. H., Lievens, K., van Bokhoven, J. A., Battiston, A. A., Weckhuysen, B. M., Pierloot, K., Weckhuysen, B. M., *Chem. Phys. Chem.*, 4, 626 (2003).
42. Groothaert, M. H., van Bokhoven, J. A., Battiston, A. A., Weckhuysen, B. M., Schoonheydt, R. A., *J. Am. Chem. Soc.*, 125, 7629 (2003).
43. Groothaert, M. H., Lievens, K., Leeman, H., Weckhuysen, B. M., Schoonheydt, R.A., *J. Catal.*, 220, 500 (2003).